HHS Public Access

Author manuscript

Oncogene. Author manuscript; available in PMC 2015 October 09.

Published in final edited form as:

Oncogene. 2015 April 9; 34(15): 1928–1937. doi:10.1038/onc.2014.147.

Effects of Tumor Suppressor Lysyl Oxidase Propeptide on Prostate Cancer Xenograft Growth and Its Direct Interactions with DNA Repair Pathways

Manish V. Bais[1], **Gokhan Baris Ozdener**[1], **Gail E. Sonenshein**[2], and **Philip C. Trackman**[1,*]

[1]Boston University Henry M. Goldman School of Dental Medicine, Department of Periodontology and Oral Biology, Boston, MA 02118

[2]Tufts University School of Medicine, Department of Biochemistry, Boston, MA 02111

Abstract

Lysyl oxidase (LOX) is a multifunctional protein required for normal collagen and elastin biosynthesis and maturation. In addition, LOX has complex roles in cancer in which the lysyl oxidase propeptide (LOX-PP) domain of secreted pro-LOX has tumor suppressor activity, while the active enzyme promotes metastasis. In prostate cancer cell lines, recombinant LOX-PP (rLOX-PP) inhibits the growth of PC3 cells in vitro by mechanisms which were not characterized, while in DU145 cells rLOX-PP targeted FGF signaling. Because rLOX-PP can enhance effects of a genotoxic chemotherapeutic on breast cancer cell apoptosis, we reasoned that rLOX-PP could target DNA repair pathways typically elevated in cancer. Here we demonstrate for the first time that rLOX-PP inhibits prostate xenograft growth *in vivo* and that activating phosphorylations of the key DNA repair molecules ATM and CHK2 are inhibited by rLOX-PP expression *in vivo*. In addition, *in vitro* studies showed that rLOX-PP inhibits radiation induced activating phosphorylations of ATM and CHK2, and that exogenously added rLOX-PP protein can localize to the nucleus in both DU145 and PC3 cells. rLOX-PP pull-down studies resulted in detection of a protein complex with the nuclear DNA repair regulator MRE11 in both cell lines, and rLOX-PP localized to radiation-induced nuclear DNA repair foci. Finally, rLOX-PP was shown to sensitize both DU145 and PC3 cells to radiation-induced cell death determined in colony formation assays. These data provide evidence that rLOX-PP has a nuclear mechanism of action in which it directly interacts with DNA repair proteins to sensitize prostate cancer cells to the effects of ionizing radiation.

Keywords

lysyl oxidase; tumor suppressor; radiation sensitivity; MRE11; colony formation; DNA repair foci

*Corresponding Author Philip C. Trackman, Ph.D. Professor, Boston University, Henry M. Goldman School of Dental Medicine, 700 Albany Street; W-201, Boston, MA 02118, trackman@bu.edu Telephone: (617) 638-4076.

All authors declare that they have no conflicts of interest regarding the contents of this manuscript.

Conflict of Interest

The authors declare that they have no conflicts of interest.

Introduction

The lysyl oxidase (*LOX*) gene has been shown to have “RAS recision” activity (Contente et al., 1990; Kenyon et al., 1991). LOX is synthesized and secreted as a 50 kDa proenzyme, and is then processed extracellularly to a ~30 kDa mature LOX enzyme and an ~18 kDa lysyl oxidase propeptide (LOX-PP) by procollagen C-proteinases (1, 2) The active enzyme is essential for biosynthetic collagen cross-linking, while the propeptide of LOX (LOX-PP) is a tumor growth inhibitor and has multiple mechanisms of action. Interestingly, active lysyl oxidase enzymes promote invasiveness in metastasis (3), but the unique propeptide region of LOX in particular acts as a tumor suppressor (4–6). Recombinant LOX-PP (rLOX-PP) has Ras recision activity and inhibits breast, prostate and lung cancer cell growth (7–9) and was recently shown to also inhibit Ewing sarcoma and hepatocellular carcinoma cell growth (10, 11). Purified rLOX-PP protein inhibits tumor growth after both direct intratumoral injection and by a slow release formulation in Her2/neu breast cancer cell xenografts (12). Thus, rLOX-PP is now understood to have therapeutic potential. In prostate cancer cells, we have shown *in vitro* that rLOX-PP inhibits FGF-2/FGF receptor-1 (FGFR1) interaction via an extracellular mechanism resulting in attenuated RAS/ERK/AKT signaling in DU145 prostate cancer cells (8). However, mechanisms of action by which rLOX-PP inhibits PC3 prostate cancer cell growth are not well characterized (8). Separate studies indicate that rLOX-PP can enhance apoptosis of breast and pancreatic cancer cell lines in the presence of doxorubicin, but not in the absence of doxorubicin (7). Because the mechanisms of action of doxorubicin include increased DNA damage (13), we reasoned that rLOX-PP could interact with or target DNA repair pathways which are elevated in cancer and which prevent mitotic catastrophe (14).

DNA damage in cells activates a complex DNA damage response (DDR). This response normally coordinates cell cycle progression with DNA repair to maintain genomic stability. Defects in the DDR cascade can inhibit cell cycle checkpoints, decrease repair responses and increase sensitivity to ionizing radiation (IR) and genotoxic chemotherapeutic agents. In response to DNA damage, a protein complex which contains MRE11, RAD50, and NBS1 (MRN complex) binds to and activates ATM protein kinase which initiates a downstream signal transduction cascade essential for coordinating cell cycle progression with DNA repair. The elevated ability to repair DNA is a characteristic of tumor cells even in the absence of acute radiation, enabling continued proliferation and dissemination. Moreover, overexpression of key DNA repair enzymes results in increased cancer cell invasiveness and tumor formation (15, 16). Chemotherapeutic inhibition of DNA damage repair responses is, therefore, an effective strategy to inhibit tumor growth with or without accompanying radiation therapy.

The present report shows that ectopic overexpression of rLOX-PP inhibits prostate cancer xenograft growth in both PC3 and DU145 cells. rLOX-PP inhibited IR-induced activating phosphorylations of ATM and CHK2, and increased DNA fragmentation. rLOX-PP was observed to be taken up by PC3 and DU145 cells with accumulation in nuclei. Moreover, rLOX-PP co-localized with repair foci and formed protein complexes with MRE11, and sensitized prostate cancer cells to IR. These data strongly suggest that one mechanism of action of rLOX-PP is to target DNA repair pathways. Thus, we propose that rLOX-PP or a

derivative could have the potential to be used in conjunction with radiation and/or genotoxic cancer therapy.

Results

Ectopic overexpression of LOX-PP inhibits mouse prostate cancer subcutaneous xenografts

Previous studies have shown that rLOX-PP inhibits prostate cancer cell growth in vitro (8). Here we hypothesize that rLOX-PP could inhibit the growth of prostate cancer cell lines by targeting DNA repair pathways. This idea is based on the finding that rLOX-PP enhances inhibition of cancer cell growth by a genotoxic agent (7), and on reports indicating that DNA repair pathways are elevated in cancer and promote metastasis (15–17). In order to first evaluate whether rLOX-PP can inhibit prostate cancer cell growth in vivo, we created xenografts in nude mice with PC3 cells and DU145 cells, respectively. PC3 and DU145 cells were stably transduced with rLOX-PP expressing- or Empty lentivirus (Materials and Methods and Figure 1A). Figure 1B shows that growth of DU145 xenografts was slower in rLOX-PP expressing xenografts compared to controls, and that tumor weight at sacrifice was 50% of control tumors (Figure 1C). PC3 xenografts expressing rLOX-PP grew slower than corresponding controls (Figure 1D), with smaller tumors observed at sacrifice (Figure 1E). Data indicate that ectopic expression of rLOX-PP inhibits tumor growth by at least 50% compared to empty vector controls. These findings demonstrate that prostate cancer xenografts are responsive to rLOX-PP in vivo.

ATM is a master regulator of double strand break repair. It auto-phosphorylates Ser1981 after binding to the MRN complex of proteins (18). Active phosphorylated ATM is a signaling kinase which phosphorylates a variety of downstream effectors including CHK2 that limits the cell cycle and/or promotes apoptosis (19). Activating phosphorylations of both ATM and CHK2 from protein extracts obtained from xenografts were measured. Figure 1F shows that ATM and CHK2 phosphorylations were inhibited by overexpression of rLOX-PP in tumor xenografts, particularly in PC3-derived xenografts.

In vitro radiation induced ATM and CHK2 phosphorylations and rLOX-PP

We next evaluated whether rLOX-PP could inhibit IR-stimulated DNA repair pathways in vitro. Radiation therapy induces a DDR response and inhibition of this response in cancer cells by chemotherapeutics is an effective anticancer therapeutic strategy (16). ATM is activated by IR and its phosphorylation of CHK2 on Thr68 initiates a phosphorylation cascade that promotes the full activity of Chk2 and cell cycle arrest (20). Thus, DU145 and PC3 cells transduced to express rLOX-PP, and empty vector transduced cells, were subjected to 5 Gy IR for different time intervals. Cell proteins were extracted for Western blotting for phosphorylated ATM (Figure 2) and phosphorylated CHK2 (Figure 3). Data show that cells expressing rLOX-PP exhibited significantly reduced levels of both ATM- and CHK2 phosphorylation after 10 min and 1 hr of radiation exposure.

To determine whether rLOX-PP expression actually resulted in increased radiation-induced DNA damage, genomic DNA was isolated from irradiated cells and subjected to agaorse gel

electrophoresis to assess for DNA fragmentation levels. Data in Figure 3E clearly show that rLOX-PP expression results in increased DNA damage.

rLOX-PP inhibition of DNA repair and RAS signaling

It has been previously reported that rLOX-PP inhibits RAS-dependent signaling (6). To investigate whether the ability of rLOX-PP to inhibit DNA repair induced by IR is mediated by RAS-dependent signaling, we assessed changes in ERK1/2 and AKT activation as a function of rLOX-PP expression in IR-treated and control DU145 and PC3 cells. Data in Figure 4 indicate that IR-induced ERK1/2 and AKT activation are not inhibited in cells expressing rLOX-PP. These data suggest that LOX-PP inhibition of IR-induced DNA damage is not primarily the result of its inhibition of IR-induced RAS signaling.

rLOX-PP nuclear localization in DU145 and PC3 cells

In order to evaluate whether rLOX-PP can internalize into the cytoplasm and ultimately into the cell nucleus of prostate cancer cells to directly target DDR response proteins, we covalently labeled biologically active rLOX-PP protein that contains a C-terminal-myc-His_6 tag with ATTO565. The ATTO565 molecule (4-[4- (dimethylamino)phenylazo]benzoic acid) is a highly sensitive red fluorescent dye that is resistant to photo-bleaching (21). rLOX-PP contains no cysteine and a one lysine residue located in the C-terminal myc-His_6 tag, and none are present in LOX-PP itself (22). rLOX-PP was, therefore, labeled with ATTO565 as described in Materials and Methods. Incubation of cells with 4 μg/ml – rLOXPP-ATTO565 for 36 hours followed by confocal immunofluorescence microscopy and analyses of Z-stack images revealed nuclear association of rLOX-PP in both DU145 and PC3 cells (Figure 5A and 5B).

rLOX-PP interacts with the MRN complex protein MRE11

If rLOX-PP directly inhibits DNA repair, it can be expected to bind one or more component of the MRN complex in its mechanism of action. We, therefore, studied direct binding of rLOX-PP with DNA repair proteins by pull down assays employing PC3 and DU145 cells transduced to express rLOX-PP or control empty vector. Cell extracts were incubated with non-immune IgG or anti-c-Myc tag IgG covalently attached to agarose beads (Pierce). Beads were washed and rLOX-PP containing protein complexes were eluted and analyzed as described in the Materials and Methods and Figure 5. The data show that rLOX-PP has specific direct or indirect interactions with MRE11 in PC3 and DU145 cells (Figure 5C and 5D) but not with ATR, Rad 50 or NBS1 (data not shown). MRE11 is a component of the MRN complex (18), and ATM binds to and is activated by the MRN complex. These findings point to the likelihood that rLOX-PP inhibits DNA repair pathways by binding to components of the DNA DSB repair complex.

rLOX-PP is present in DNA damage induced repair foci

Histone H2AX is a substrate of ATM kinase to form phosphorylated-H2AX, which is a component and excellent marker of the DNA double strand break repair complex and of DNA repair foci (23, 24). Next we asked whether rLOX-PP is a component of IR-induced repair foci. rLOX-PP-ATTO565 treated PC3- and DU145 cells were irradiated with 5 Gy

IR, and then stained for phosphorylated-H2AX and MRE11 (Materials and Methods). Figure 6 shows that IR increased the presence of repair foci, and that rLOX-PP co-localized with phosphorylated-H2AX, and MRE11-containing nuclear foci.

rLOX-PP inhibits clonogenic survival in response to radiation

Based on these data we predicted that LOX-PP would sensitize PC3 and DU145 cells to ionizing radiation. Cells expressing rLOX-PP or transduced with empty lentivirus were subjected to different doses of IR. Live cells were sorted by flow cytometry and were plated. Colonies were allowed to grow for 2 weeks (Materials and Methods). DU145 and PC3 cells expressing rLOX-PP resulted in fewer colonies at all doses of IR compared to empty cells (Figure 7). Correcting for plating efficiency determined at 0 Gy, the surviving fraction in rLOX-PP expressing cells was significantly diminished compared to the empty control ($p<0.001$); and the size of colonies was smaller in the rLOX-PP expressing cells (Figure 7). rLOX-PP significantly decreased colonies in the prostate cancer cells treated with 1–2 Gy IR. This finding shows that rLOX-PP is effective at sensitizing cancer cells *in vitro* to radiation at clinically relevant doses used in radiation therapy *in vivo*. (25).

Discussion

Biologic chemotherapeutics which inhibit a single specific pathway and are effective in the short term are often not effective to treat cancer in the long term due to development of drug resistance and robust relapse (26–29). Up-regulation of DNA repair pathways is one way in which tumor cells become resistant to therapy and through which mitotic catastrophe is avoided in damaged tumor cells (14). In our opinion, there is a place for derivatives of biomolecules which can inhibit tumor growth by multiple mechanisms of action and which would have therapeutic value with low toxicity. Such agents could be used in conjunction with more conventional chemotherapeutic and/or radiation protocols and could reduce the dosing requirements of the harsher therapeutics. rLOX-PP inhibits tumor growth by several mechanisms of action and targets both cell surface receptors and intracellular signaling molecules (4, 8, 12, 30–34). rLOX-PP tumor inhibitory properties are mediated by inhibiting RAS, FGFR1, β-catenin activation, and/or FAK signaling. Although rLOX-PP inhibits serum-induced stimulation in both DU145 and PC3 cells, this activity is mediated by FGF-2/FGFR1 signaling in DU145 cells and not in PC3 cells.

As noted, DNA repair pathways are often up-regulated in cancer cells to help avoid mitotic catastrophe (14). The protein kinase ataxia-telangiectasia mutated (ATM) is an apical activator of the DNA damage response at DNA double-strand breaks (DSBs) (35). The MRN complex is required for optimal ATM activation at DSBs (36), and is one of the first complexes to be recruited to DSB sites, where it acts as a damage sensor that can also form a physical bridge spanning the DSB ends. It is required for timely repair by both non-homologous end-joining (NHEJ) and homology-directed repair (HDR). MRE11 takes part in DSB end resection, which is essential for homologous DNA repair (35). The interaction of ATM with the MRN complex initiates a highly coordinated program of further recruitment of DNA damage response proteins including MDC1 (Mediator of DNA Damage Checkpoint Protein 1) and other proteins to sites of DSB repair (37). rLOX-PP robust inhibition of ATM

and CHK2 phosphorylation in xenografts grown in mice even without radiation treatment suggests that DNA repair pathways could be a target of rLOX-PP in these cells. Inhibition by rLOX-PP of both ATM and CHK2 phosphorylation and reduced colony formation occurred after IR in vitro in both cell lines. These data suggest that rLOX-PP inhibition of DNA repair pathways can occur in both cell lines. ATM activity inhibition enhances the sensitivity of tumor cells to the cytotoxic effects of IR and to sensitizing chemotherapeutic agents (38–40). The downstream target of ATM is CHK2 which causes cell cycle arrest and provides cells time to repair DNA. Selective CHK1 and CHK2 inhibitors such as 7-hydroxystaurosporine (UCN-01), aminopyrazine XL844, AZD7762 (a thiophene urea carboxamide) are in clinical trials to inhibit tumor growth (41). CHK2-specific inhibitors as isothiazole carboximidamine, VRX046617, and the bis-guanylhydrazone NSC 109555 have been identified to target DNA damage repair pathways in cancer cells (42, 43). In our studies, rLOX-PP inhibits activating phosphorylation of CHK2 in both of the two androgen-independent prostate cancer cell lines examined.

rLOX-PP can enter nuclei and forms complexes with MRE11 in both PC3 and DU145 cells. In DSB repair complexes, ATM, MRE11 and phosphorylated-H2AX are present in DNA repair foci. MRE11 is the core of the MRN complex and interacts with both RAD50 and NBS1 (44–46). Further, in mammalian cells the MRE11 complex mediates the S-phase checkpoint through an interaction with replication protein A (47). Our data suggest that rLOX-PP disrupts productive functional interactions involved in the MRN complexes resulting in inhibited downstream signaling required for DNA repair. Moreover, MRE11 is a nuclease which has a role in DNA splicing in DSB repair (48). MRE11 is a conserved protein with an N-terminal nuclease domain (49, 50) and a DNA-binding region (51, 52) encompassing the glycine-arginine motif which is predicted to regulate DNA double-strand break processing (53). Further studies are required to determine whether or not MRE11 is a direct binding partner for rLOX-PP in its ability to inhibit the DSB repair response.

rLOX-PP was localized to phosphorylated-H2AX- and MRE11-containing DNA damage-induced foci which confirms that rLOX-PP binds to DSB complexes. In order to arrest cell cycle progression at sites containing damaged chromatin, phosphorylated-H2AX is required for the assembly of DNA repair protein complexes and for activation of checkpoint proteins. H2AX-containng nuclear foci are used to detect genotoxic effects and to monitor the efficiency of anticancer treatment to predict of tumor cell sensitivity to gentotoxic anticancer agents (54). H2AX becomes extensively phosphorylated within three minutes of DNA damage, forms foci at break sites and recruits other factors at foci. The product of the tumor suppressor gene BRCA1 also co localizes with phosphorylated-H2AX and is recruited to these sites before Rad50 or Rad51 (55).

In summary, rLOX-PP sensitizes cells to ionizing radiation in clonogenic survival assays at clinically relevant doses of IR in both PC3 and DU145 cell lines. Clinically in prostate cancer patients, conventionally fractionated external beam radiation therapy uses 1.8 – 2.0 Gy/fraction. (56). Moreover, rLOX-PP interferes with the DSB repair response in cancer cells by inhibiting ATM and CHK2 phosphorylation. rLOX-PP interacts with MRE11 and H2AX foci. Thus, we propose that a mechanism of action of the rLOX-PP effect is through its interaction with the MRN complex, and inhibition of DSB repair signaling. This study

raises the novel concept that rLOX-PP, or a derivative, could be used in combination with radiation therapy and/or with genotoxic drugs, increasing the effectiveness of these conventional therapies. Evaluation of the responsiveness of rLOX-PP in pre-clinical orthotropic mouse models in combination with DNA damaging agents including radiation and/or DNA-directed chemotherapeutic drugs is now of considerable interest.

Materials and Methods

Mouse xenografts

All in vivo experiments were approved by Boston University Medical Center IACUC. PC3 and DU145 cells were stably transduced with rLOX-PP expressing lentivirus particles EF1α-LOX-PP-myc-his-UBC-GFP (designated as rLOX-PP) and empty vector EF1α-Empty-UBC-GFP (designated as Empty). Cells transduced with rLOX-PP- or Empty constructs (4×10^6 cells) were respectively injected subcutaneously into the midline dorsa (n = 5) of NCR nu/nu mice (Taconic Farms, Hudson, NY) as single cell suspensions in serum-free DMEM. Caliper measurements were performed at regular intervals to monitor the volumes of all tumors. Tumors were harvested at sacrifice, weighed and snap frozen, ground to a fine powder in liquid nitrogen and then extracted for Western blotting.

Western blots

Tumor samples or cell layers were extracted into SDS PAGE sample buffer (0.1 mM Tris-HCl, 4% SDS, 10% glycerol, 5% β-mercaptoethanol) and boiled for three to five minutes. Cell culture media samples were boiled after adding one volume of 2X SDS PAGE sample buffer. Protein concentrations were determined using Nano Orange assay kits (Molecular Probes, Eugene, OR). From tumors, approximately 40 micrograms of protein from 3 tumors per experimental group were then subjected to 6% or 10% SDS PAGE and Western blotting with primary antibodies from Cell Signaling Technology (Danvers, MA). The antibodies used were phospho-ATM (#5883), ATM (#2873), phospho-CHK2 (#2661), CHK2 (#2662) and MRE11 (#4895) and normalization control β-actin (#4970). LOX-PP antibody was prepared as described earlier (8). Anti-rabbit and anti-mouse secondary antibodies were purchased from Cell Signaling Technology (Danvers, MA; 7074 and 7076, respectively). The quantifications were performed by a digital densitometry system (Versadoc; BioRad, Hercules, CA) and Image J software.

In vitro radiation protocol for ATM and CHK2 activation

PC3 and DU145 cells expressing rLOX-PP or empty vector controls were plated and grown in DMEM/F12K media with 10% serum under standard conditions. Cells were transduced with the rLOX-PP or empty lentivirus particles and plated in 6-well plates (57). At 80% visual confluence, cells were placed in serum-free medium overnight. Cultures (n = 3) were then irradiated with 5 Gy IR with a [^{137}Cs] γ-irradiator. Cells were cultured for an additional 10 min, 1 hr and 6 hrs and cell layers were collected as described above in SDS PAGE sample buffer and were subjected to Western blot analysis.

rLOX-PP labeling and localization to cell nuclei

rLOX-PP uptake studies were performed by labeling rLOX-PP at the N-terminus and at the only lysine residue which is located in the C-terminal myc-His_6 tag employing the N-hydrosuccinamide ester of ATTO565 (4-[4-(dimethylamino)phenylazo]benzoic acid) (Molecular Probes, Eugene, OR). rLOX-PP (2 mg/ml) in 0.1 M sodium bicarbonate buffer (pH=8.3) was treated with a 10-fold molar excess of ATTO565-NHS ester and incubated at 37°C for 3 hrs, followed by incubation at 4°C overnight (58, 59). The samples were diluted with 200 mM sodium phosphate buffer, 10 M urea (pH 7.8) resulting in a final urea concentration of 4 M. In order to remove unlabeled dye, the sample was subjected to gel filtration chromatography through a Sephadex G-25 column (GE Healthcare, Waukesha, WA, PD MiniTrap™ G-25, #28-9180-07). The column was pre-equilibrated with 200 mM sodium phosphate buffer with 10 M urea (pH 7.8) and eluted with same buffer at room temperature. The flow-through fraction containing rLOX-PP–ATTO565 was collected. Labeled rLOX-PP was then dialyzed against water using 10,000 Dalton molecular weight cut off Slide-A-Lyzer dialysis cassettes (Thermo Scientific, Waltham, MA). To confirm that free dye was removed, samples were subjected to 12% SDS-PAGE gel and compared to the mobility of free ATTO565 dye and imaged (Ex 565 nm, Em 592 nm) with a Molecular Imager FX (Biorad, Hercules, CA). The stoichiometry of ATTO565 labeling of rLOX-PP was calculated based on extinction coefficients of rLOX-PP and ATTO565 (Molecular Probes, Eugene, OR). The extinction coefficient of ATTO565 is 120,000 L mol^{-1} cm^{-1} (563 nm) and rLOX-PP is 19,480 L mol^{-1} cm^{-1} (280 nm). Uptake studies were performed in live cells by plating 30,000 PC3 and DU145 cells in F12K or DMEM media (10% FBS, 1% penicillin-streptomycin) in chamber slides, respectively, and cultured overnight. The cells were replenished with serum-free F12K or DMEM media containing 0.1% BSA, and 1% penicillin-streptomycin for 24 hrs. rLOX-PP-ATTO565 was then added as indicated and incubated for another 36 hrs. The cells were imaged with a Zeiss 710 dual scanner confocal microscope as indicated.

DNA fragmentation assay

In order to determine the direct physical effect of LOX-PP on IR induced DNA damage, a DNA fragmentation assay was performed (60). Empty vector and rLOX-PP expressing PC3 and DU145 cells were cultured and treated with IR (5 Gy). After 24 hr, cells were lysed in 0.2% Triton X-100; 10 mM Tris-HCl, pH 7.4, 10 mM EDTA. Samples were centrifuged and supernatants extracted with phenol:chloroform:isoamyl alcohol (25:24:1) followed by chloroform:isoamyl alcohol (24:1) twice. DNA was precipitated by adding of 5 M NaCl to a final concentration of 300 mM and 2.5 volume of ice-cold 100% ethanol, washed with 70% ethanol, dried and suspended in 10 mM Tris-HCl, pH7.5, 1 mM EDTA. DNA samples (25 μg each) were subjected to 2% agarose gel electrophoresis analysis.

rLOX-PP Pull down assays

Empty vector and rLOX-PP expressing PC3 and DU145 cells were cultured, extracted into non-denaturing RIPA cell lysis buffer and incubated with agarose bead-immobilized non-immune IgG or anti-c-Myc tag IgG overnight at 4°C to pull down rLOX-PP. Non-immune IgG (#31903, Thermo Scientific, Waltham, MA) was coupled to agarose using AminoLink

Immobilization Plus Trial kit (#20394, Thermo Scientific, Waltham, MA) according to the manufacturer's instructions. For pull-down assays, beads were washed, and then eluted according to kit instructions (ProFound c-Myc Tag IP/Co-IP Kit; Thermo Scientific, Waltham, MA). Eluted samples were analyzed by Western blotting on denaturing SDS PAGE probed with an anti-ATM, anti-ATR, Rad50, anti-NBS1 and anti-MRE11 antibodies (Cell Signaling, Danvers, MA) and with anti-rLOX-PP antibody (61). Aliquots (5%) of initial extracts taken before the immunoprecipitation were analyzed by Western blot on the same gels.

Foci formation assay

DU145 and PC3 cells were respectively plated in chamber slides and cultured for 18 hrs in standard media with serum. Cells were incubated for an additional 36 hrs in serum-free media supplemented with rLOX-PP-ATTO565 at 10 μg/ml, or vehicle. After incubation, the cells were subjected to IR (5 Gy) and allowed to recover for 1 hr. The cells were fixed with 4% paraformaldehyde for 10 min and blocked with blocking buffer (1X PBS/5% normal rabbit serum/0.3% Triton™ X-100) for 1 hr. Cells were incubated with anti-MRE 11 antibody (Cell Signaling, Danvers, MA, #4895) or rabbit non-immune control IgG (1.1 μg/ml) in 1X PBS, 1% BSA, 0.3% Triton™ X-100) for 2 hrs. Cells were washed and treated with Alexa Fluor 647 conjugated anti-rabbit IgG (Molecular Probes, Eugene, OR, #4414; 400 μg/ml) to respective samples, and incubated for an additional 1 hr and were extensively washed 3 times with PBS. Samples were then incubated with rabbit IgG non-immune control antibody and incubated for 1 hr at room temperature in the dark. This step blocks any remaining free Alexa Fluor 647 labeled anti-rabbit secondary antibody for the subsequent step. Finally, anti-phosphohistone H2AX rabbit mAb (Cell Signaling, Danvers, MA, #9719) or its isotype control (Cell Signaling, Danvers, MA, #2975), each directly conjugated with Alexa Fluor 488 in antibody dilution buffer (1X PBS/1% BSA/0.3% Triton™ X-100), were added in respective samples and incubated for 2 hr at room temperature in the dark. Anti-fade reagent with DAPI was added to all the samples and imaged. A Zeiss 710 dual scanner confocal microscope with a Plan-Apochromat objective, oil immersion lens and a CCD detector was used to obtain confocal images. Image acquisition was performed with Zeiss Zen image analysis software (Carl Zeiss Micro Imaging, Inc., Thornwood, NY). The image analysis was performed using Zeiss LSM viewer and Image J software (NIH, USA). Z-stack images analysis and 3-dimensional reconstruction was performed by using LOCI and the 3D viewer plug-in of Image J software.

Clonogenic survival assay

Empty vector and rLOX-PP expressing DU145 and PC3 cells were plated and grown in DMEM and 10% serum under standard conditions in 6-well plates. At 80% visual confluence, cells were placed in serum-free medium overnight. Cells expressing rLOX-PP and their respective controls (n=6) were then irradiated and then plated in 6-well plates as follows. Cells were trypsinized and subjected to sorting (Aria FACS, BioRad, Hercules, CA). The cell sorting was performed to exclude dead cells due to IR treatment by utilizing the Near-IR dead cell stain kit (Invitrogen Inc., Carlsbad, CA). The number of cells needed for successful initial plating of 5,000 and 10,000 cells per well in 6-well plates was

determined based on the plating efficiency determined at 0 Gy. The clonogenic survival assay, calculation of plating efficiency and the survival fraction determinations were performed as described (62, 63). Colonies were allowed to grow for 14 days, and cultures were then fixed, and stained with crystal violet and colony numbers were determined using a Versadoc Photodocumentation System and Quantity One colony counting software (BioRad, Hercules, CA). The survival fraction was calculated and plotted as described (62).

Statistical analysis

Analyses of all experiments were done using two way ANOVA with Bonferroni post-hoc analysis or Student's t-test (Graph Pad Prism 5 software, La Jolla, CA) as indicated in Figure legends. All experiments were performed at least three times.

Acknowledgments

Supported by NIH grants DE R01014066, DOD W81XWH-08-1-0349 PC073646, and R01 CA143108.

References

1. Panchenko MV, Stetler-Stevenson WG, Trubetskoy OV, Gacheru SN, Kagan HM. Metalloproteinase activity secreted by fibrogenic cells in the processing of prolysyl oxidase. Potential role of procollagen C-proteinase. The Journal of biological chemistry. 1996; 271(12): 7113–9. [PubMed: 8636146]
2. Uzel MI, Scott IC, Babakhanlou-Chase H, Palamakumbura AH, Pappano WN, Hong HH, et al. Multiple bone morphogenetic protein 1-related mammalian metalloproteinases process pro-lysyl oxidase at the correct physiological site and control lysyl oxidase activation in mouse embryo fibroblast cultures. The Journal of biological chemistry. 2001; 276(25):22537–43. [PubMed: 11313359]
3. Barker HE, Cox TR, Erler JT. The rationale for targeting the LOX family in cancer. Nature reviews Cancer. 2012; 12(8):540–52. [PubMed: 22810810]
4. Min C, Kirsch KH, Zhao Y, Jeay S, Palamakumbura AH, Trackman PC, et al. The tumor suppressor activity of the lysyl oxidase propeptide reverses the invasive phenotype of Her-2/neu-driven breast cancer. Cancer research. 2007; 67(3):1105–12. [PubMed: 17283144]
5. Min C, Yu Z, Kirsch KH, Zhao Y, Vora SR, Trackman PC, et al. A loss-of-function polymorphism in the propeptide domain of the LOX gene and breast cancer. Cancer research. 2009; 69(16):6685–93. [PubMed: 19654310]
6. Palamakumbura AH, Jeay S, Guo Y, Pischon N, Sommer P, Sonenshein GE, et al. The propeptide domain of lysyl oxidase induces phenotypic reversion of ras-transformed cells. The Journal of biological chemistry. 2004; 279(39):40593–600. [PubMed: 15277520]
7. Min C, Zhao Y, Romagnoli M, Trackman PC, Sonenshein GE, Kirsch KH. Lysyl oxidase propeptide sensitizes pancreatic and breast cancer cells to doxorubicin-induced apoptosis. Journal of cellular biochemistry. 2010; 111(5):1160–8. [PubMed: 20717927]
8. Palamakumbura AH, Vora SR, Nugent MA, Kirsch KH, Sonenshein GE, Trackman PC. Lysyl oxidase propeptide inhibits prostate cancer cell growth by mechanisms that target FGF-2-cell binding and signaling. Oncogene. 2009; 28(38):3390–400. [PubMed: 19597471]
9. Wu M, Min C, Wang X, Yu Z, Kirsch KH, Trackman PC, et al. Repression of BCL2 by the tumor suppressor activity of the lysyl oxidase propeptide inhibits transformed phenotype of lung and pancreatic cancer cells. Cancer research. 2007; 67(13):6278–85. [PubMed: 17616686]
10. Agra N, Cidre F, Garcia-Garcia L, de la Parra J, Alonso J. Lysyl oxidase is downregulated by the EWS/FLI1 oncoprotein and its propeptide domain displays tumor supressor activities in ewing sarcoma cells. PloS one. 2013; 8(6):e66281. [PubMed: 23750284]

11. Zheng Y, Wang X, Wang H, Yan W, Zhang Q, Chang X. Expression of the lysyl oxidase propeptide in hepatocellular carcinoma and its clinical relevance. Oncol Rep. 2014; 31(4):1669–76. [PubMed: 24573150]
12. Bais MV, Nugent MA, Stephens DN, Sume SS, Kirsch KH, Sonenshein GE, et al. Recombinant lysyl oxidase propeptide protein inhibits growth and promotes apoptosis of pre-existing murine breast cancer xenografts. PloS one. 2012; 7(2):e31188. [PubMed: 22363577]
13. Spalding AC, Jotte RM, Scheinman RI, Geraci MW, Clarke P, Tyler KL, et al. TRAIL and inhibitors of apoptosis are opposing determinants for NF-kappaB-dependent, genotoxin-induced apoptosis of cancer cells. Oncogene. 2002; 21(2):260–71. [PubMed: 11803469]
14. Curtin NJ. DNA repair dysregulation from cancer driver to therapeutic target. Nature reviews Cancer. 2012; 12(12):801–17. [PubMed: 23175119]
15. Sarasin A, Kauffmann A. Overexpression of DNA repair genes is associated with metastasis: a new hypothesis. Mutation research. 2008; 659(1–2):49–55. [PubMed: 18308619]
16. Kauffmann A, Rosselli F, Lazar V, Winnepenninckx V, Mansuet-Lupo A, Dessen P, et al. High expression of DNA repair pathways is associated with metastasis in melanoma patients. Oncogene. 2008; 27(5):565–73. [PubMed: 17891185]
17. Martinez-Marignac VL, Rodrigue A, Davidson D, Couillard M, Al-Moustafa AE, Abramovitz M, et al. The effect of a DNA repair gene on cellular invasiveness: XRCC3 over-expression in breast cancer cells. PloS one. 2011; 6(1):e16394. [PubMed: 21283680]
18. Lee JH, Paull TT. Direct activation of the ATM protein kinase by the Mre11/Rad50/Nbs1 complex. Science. 2004; 304(5667):93–6. [PubMed: 15064416]
19. Stolz A, Ertych N, Bastians H. Tumor suppressor CHK2: regulator of DNA damage response and mediator of chromosomal stability. Clinical cancer research : an official journal of the American Association for Cancer Research. 2011; 17(3):401–5. [PubMed: 21088254]
20. Buscemi G, Carlessi L, Zannini L, Lisanti S, Fontanella E, Canevari S, et al. DNA damage-induced cell cycle regulation and function of novel Chk2 phosphoresidues. Molecular and cellular biology. 2006; 26(21):7832–45. [PubMed: 16940182]
21. Berlier JE, Rothe A, Buller G, Bradford J, Gray DR, Filanoski BJ, et al. Quantitative comparison of long-wavelength Alexa Fluor dyes to Cy dyes: fluorescence of the dyes and their bioconjugates. J Histochem Cytochem. 2003; 51(12):1699–712. [PubMed: 14623938]
22. Vora SR, Guo Y, Stephens DN, Salih E, Vu ED, Kirsch KH, et al. Characterization of recombinant lysyl oxidase propeptide. Biochemistry. 2010; 49(13):2962–72. [PubMed: 20192271]
23. Delia D, Fontanella E, Ferrario C, Chessa L, Mizutani S. DNA damage-induced cell-cycle phase regulation of p53 and p21waf1 in normal and ATM-defective cells. Oncogene. 2003; 22(49): 7866–9. [PubMed: 14586414]
24. Bakkenist CJ, Kastan MB. DNA damage activates ATM through intermolecular autophosphorylation and dimer dissociation. Nature. 2003; 421(6922):499–506. [PubMed: 12556884]
25. Ritter M. Rationale, conduct, and outcome using hypofractionated radiotherapy in prostate cancer. Semin Radiat Oncol. 2008; 18(4):249–56. [PubMed: 18725112]
26. Oxnard GR. Strategies for overcoming acquired resistance to epidermal growth factor receptor: targeted therapies in lung cancer. Arch Pathol Lab Med. 2012; 136(10):1205–9. [PubMed: 23020725]
27. Pallis A, Briasoulis E, Linardou H, Papadimitriou C, Bafaloukos D, Kosmidis P, et al. Mechanisms of resistance to epidermal growth factor receptor tyrosine kinase inhibitors in patients with advanced non-small-cell lung cancer: clinical and molecular considerations. Current medicinal chemistry. 2011; 18(11):1613–28. [PubMed: 21428885]
28. Neel DS, Bivona TG. Secrets of drug resistance in NSCLC exposed by new molecular definition of EMT. Clin Cancer Res. 2013; 19(1):3–5. [PubMed: 23172883]
29. Matos CS, de Carvalho AL, Lopes RP, Marques MP. New strategies against prostate cancer--Pt(II)-based chemotherapy. Current medicinal chemistry. 2012; 19(27):4678–87. [PubMed: 22856665]
30. Sato S, Trackman PC, Maki JM, Myllyharju J, Kirsch KH, Sonenshein GE. The Ras signaling inhibitor LOX-PP interacts with Hsp70 and c-Raf to reduce Erk activation and transformed

phenotype of breast cancer cells. Molecular and cellular biology. 2011; 31(13):2683–95. [PubMed: 21536655]

31. Sato S, Zhao Y, Imai M, Simister PC, Feller SM, Trackman PC, et al. Inhibition of CIN85-Mediated Invasion by a Novel SH3 Domain Binding Motif in the Lysyl Oxidase Propeptide. PloS one. 2013; 8(10):e77288. [PubMed: 24167568]
32. Zhao Y, Min C, Vora SR, Trackman PC, Sonenshein GE, Kirsch KH. The lysyl oxidase propeptide attenuates fibronectin-mediated activation of focal adhesion kinase and p130Cas in breast cancer cells. The Journal of biological chemistry. 2009; 284(3):1385–93. [PubMed: 19029090]
33. Palamakumbura AH, Sommer P, Trackman PC. Autocrine growth factor regulation of lysyl oxidase expression in transformed fibroblasts. The Journal of biological chemistry. 2003; 278(33): 30781–7. [PubMed: 12788924]
34. Sanchez-Morgan N, Kirsch KH, Trackman PC, Sonenshein GE. The lysyl oxidase propeptide interacts with the receptor-type protein tyrosine phosphatase kappa and inhibits beta-catenin transcriptional activity in lung cancer cells. Molecular and cellular biology. 2011; 31(16):3286–97. [PubMed: 21690299]
35. Shiloh Y, Ziv Y. The ATM protein kinase: regulating the cellular response to genotoxic stress, and more. Nat Rev Mol Cell Biol. 2013; 14(4):197–210.
36. Bhatti S, Kozlov S, Farooqi AA, Naqi A, Lavin M, Khanna KK. ATM protein kinase: the linchpin of cellular defenses to stress. Cellular and molecular life sciences : CMLS. 2011; 68(18):2977–3006. [PubMed: 21533982]
37. Mok MT, Henderson BR. Three-dimensional imaging reveals the spatial separation of gammaH2AX-MDC1-53BP1 and RNF8-RNF168-BRCA1-A complexes at ionizing radiation-induced foci. Radiotherapy and oncology : journal of the European Society for Therapeutic Radiology and Oncology. 2012; 103(3):415–20. [PubMed: 22633816]
38. Choudhury A, Cuddihy A, Bristow RG. Radiation and new molecular agents part I: targeting ATM-ATR checkpoints, DNA repair, and the proteasome. Semin Radiat Oncol. 2006; 16(1):51–8. [PubMed: 16378907]
39. Eastman A. Cell cycle checkpoints and their impact on anticancer therapeutic strategies. Journal of cellular biochemistry. 2004; 91(2):223–31. [PubMed: 14743382]
40. Rainey MD, Charlton ME, Stanton RV, Kastan MB. Transient inhibition of ATM kinase is sufficient to enhance cellular sensitivity to ionizing radiation. Cancer research. 2008; 68(18): 7466–74. [PubMed: 18794134]
41. Lapenna S, Giordano A. Cell cycle kinases as therapeutic targets for cancer. Nat Rev Drug Discov. 2009; 8(7):547–66. [PubMed: 19568282]
42. Carlessi L, Buscemi G, Larson G, Hong Z, Wu JZ, Delia D. Biochemical and cellular characterization of VRX0466617, a novel and selective inhibitor for the checkpoint kinase Chk2. Mol Cancer Ther. 2007; 6(3):935–44. [PubMed: 17363488]
43. Jobson AG, Cardellina JH 2nd, Scudiero D, Kondapaka S, Zhang H, Kim H, et al. Identification of a Bis-guanylhydrazone [4,4′-Diacetyldiphenylurea-bis(guanylhydrazone); NSC 109555] as a novel chemotype for inhibition of Chk2 kinase. Mol Pharmacol. 2007; 72(4):876–84. [PubMed: 17616632]
44. Hopfner KP, Karcher A, Craig L, Woo TT, Carney JP, Tainer JA. Structural biochemistry and interaction architecture of the DNA double-strand break repair Mre11 nuclease and Rad50-ATPase. Cell. 2001; 105(4):473–85. [PubMed: 11371344]
45. Usui T, Ohta T, Oshiumi H, Tomizawa J, Ogawa H, Ogawa T. Complex formation and functional versatility of Mre11 of budding yeast in recombination. Cell. 1998; 95(5):705–16. [PubMed: 9845372]
46. Lee JH, Ghirlando R, Bhaskara V, Hoffmeyer MR, Gu J, Paull TT. Regulation of Mre11/Rad50 by Nbs1: effects on nucleotide-dependent DNA binding and association with ataxia-telangiectasia-like disorder mutant complexes. The Journal of biological chemistry. 2003; 278(46):45171–81. [PubMed: 12966088]
47. Olson E, Nievera CJ, Liu E, Lee AY, Chen L, Wu X. The Mre11 complex mediates the S-phase checkpoint through an interaction with replication protein A. Molecular and cellular biology. 2007; 27(17):6053–67. [PubMed: 17591703]

48. Buis J, Wu Y, Deng Y, Leddon J, Westfield G, Eckersdorff M, et al. Mre11 nuclease activity has essential roles in DNA repair and genomic stability distinct from ATM activation. Cell. 2008; 135(1):85–96. [PubMed: 18854157]

49. Williams RS, Moncalian G, Williams JS, Yamada Y, Limbo O, Shin DS, et al. Mre11 dimers coordinate DNA end bridging and nuclease processing in double-strand-break repair. Cell. 2008; 135(1):97–109. [PubMed: 18854158]

50. Paull TT, Gellert M. The 3′ to 5′ exonuclease activity of Mre 11 facilitates repair of DNA double-strand breaks. Mol Cell. 1998; 1(7):969–79. [PubMed: 9651580]

51. de Jager M, Dronkert ML, Modesti M, Beerens CE, Kanaar R, van Gent DC. DNA-binding and strand-annealing activities of human Mre11: implications for its roles in DNA double-strand break repair pathways. Nucleic Acids Res. 2001; 29(6):1317–25. [PubMed: 11238998]

52. Hopfner KP, Craig L, Moncalian G, Zinkel RA, Usui T, Owen BA, et al. The Rad50 zinc-hook is a structure joining Mre11 complexes in DNA recombination and repair. Nature. 2002; 418(6897): 562–6. [PubMed: 12152085]

53. Yu Z, Vogel G, Coulombe Y, Dubeau D, Spehalski E, Hebert J, et al. The MRE11 GAR motif regulates DNA double-strand break processing and ATR activation. Cell Res. 2012; 22(2):305–20. [PubMed: 21826105]

54. Podhorecka M, Skladanowski A, Bozko P. H2AX Phosphorylation: Its Role in DNA Damage Response and Cancer Therapy. J Nucleic Acids. 2010

55. Paull TT, Rogakou EP, Yamazaki V, Kirchgessner CU, Gellert M, Bonner WM. A critical role for histone H2AX in recruitment of repair factors to nuclear foci after DNA damage. Curr Biol. 2000; 10(15):886–95. [PubMed: 10959836]

56. Zaorsky NG, Ohri N, Showalter TN, Dicker AP, Den RB. Systematic review of hypofractionated radiation therapy for prostate cancer. Cancer Treat Rev. 2013

57. Bais MV, Wigner N, Young M, Toholka R, Graves DT, Morgan EF, et al. BMP2 is essential for post natal osteogenesis but not for recruitment of osteogenic stem cells. Bone. 2009; 45(2):254–66. [PubMed: 19398045]

58. Nakano D, Kobori H, Burford JL, Gevorgyan H, Seidel S, Hitomi H, et al. Multiphoton imaging of the glomerular permeability of angiotensinogen. Journal of the American Society of Nephrology : JASN. 2012; 23(11):1847–56. [PubMed: 22997258]

59. Wang L, Sapuri-Butti AR, Aung HH, Parikh AN, Rutledge JC. Triglyceride-rich lipoprotein lipolysis increases aggregation of endothelial cell membrane microdomains and produces reactive oxygen species. Am J Physiol Heart Circ Physiol. 2008; 295(1):H237–44. [PubMed: 18487440]

60. Matassov D, Kagan T, Leblanc J, Sikorska M, Zakeri Z. Measurement of apoptosis by DNA fragmentation. Methods Mol Biol. 2004; 282:1–17. [PubMed: 15105553]

61. Hurtado PA, Vora S, Sume SS, Yang D, St Hilaire C, Guo Y, et al. Lysyl oxidase propeptide inhibits smooth muscle cell signaling and proliferation. Biochemical and biophysical research communications. 2008; 366(1):156–61. [PubMed: 18060869]

62. Franken NA, Rodermond HM, Stap J, Haveman J, van Bree C. Clonogenic assay of cells in vitro. Nature protocols. 2006; 1(5):2315–9. [PubMed: 17406473]

63. Munshi A, Hobbs M, Meyn RE. Clonogenic cell survival assay. Methods Mol Med. 2005; 110:21–8. [PubMed: 15901923]

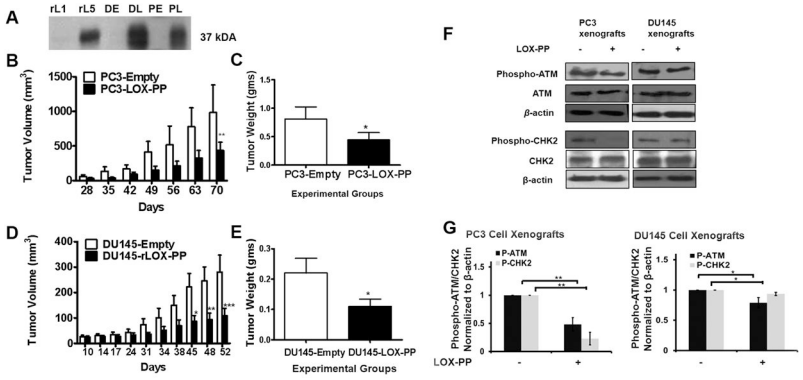

Figure 1. Ectopic overexpression of LOX-PP inhibits DU145 and PC3 xenografts growth in mice and inhibits ATM and CHK2 phosphorylation

(A) Ectopic overexpression of rLOX-PP in PC3 and DU145 cells by lentiviral transduction as described in Materials and Methods, and Western blot analysis of cell culture supernatants to evaluate LOX-PP expression. Lanes **rL1** and **rL5** are 1 and 5 ng of rLOX-PP protein as a Western blot control; lane **DE**, conditioned medium sample from DU145 cells transduced with CMV-Empty; lane **DL**, DU145 conditioned medium sample from cells transduced with rLOX-PP lentivirus; lane **PE**, conditioned medium sample from PC3 cells transduced with Empty lentivirus particles; lane **PL**, conditioned medium sample from PC3 cells transduced with rLOX-PP lentivirus; **(B)** subcutaneous murine xenografts of PC3 cells infected with Empty or rLOX-PP expressing virus as generated above. The tumor size was monitored by caliper measurements (n=5); * $p<0.05$ analysis by two way ANOVA; **(C)** tumor weight at sacrifice on day 70. **(D)** Subcutaneous murine xenografts of DU145 cells infected with Empty or rLOX-PP expressing lentivirus particles (n=5); * $p<0.05$, ** $p<0.01$, *** $p<0.001$; analysis by two way ANOVA; **(E)** tumor weight at sacrifice on day 52; **(F)** Western blot analysis of tumor extracts for ATM and CHK2 phosphorylation, total ATM and CHK2 and β-actin. Equal amounts of protein from each tumor xenograft (n=4) were pooled together and 40 μg samples were loaded to evaluate the expression of phospho-ATM/CHK2, total ATM/CHK2 and β-actin. These pooled samples were run 3 times, quantified and plotted. **(G)** Quantification and normalization of phospho-ATM and CHK2 levels from tumors derived from Western blots. Data are the averages of means of three independent experiments +/− SEM; n = 3, * $p<0.05$, ** $p<0.01$, Student's t-test.

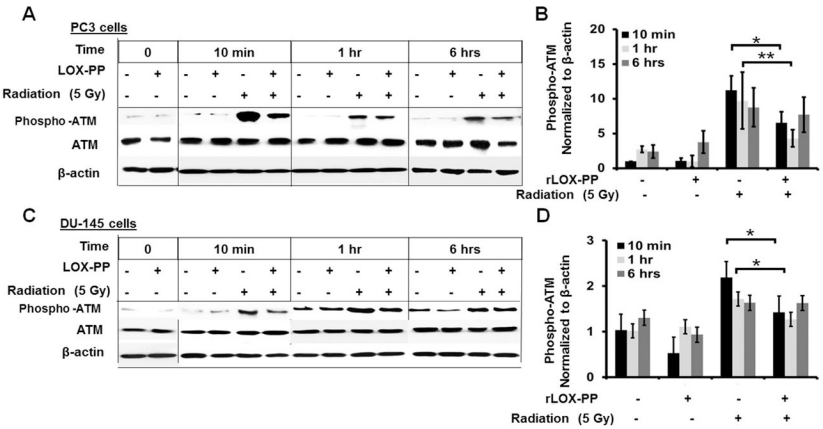

Figure 2. LOX-PP inhibits IR induced DNA damage repair response by inhibiting ATM phosphorylation

PC3 and DU145 cells transduced with Empty and rLOX-PP lentivirus particles were plated in 6-well plates and subjected to IR (5 Gy). Equal amounts of protein extracts from each cell sample (n=3) were pooled together and 40 μg samples were evaluated for the expression of phospho-ATM, total ATM and β-actin by Western blotting. The experiments were repeated with 3 different preparations of cells. **(A)** Representative Western blots for phospho-ATM, total ATM and β-actin as a loading control from PC3-Empty and PC3-LOX-PP cells subjected to IR (5 Gy) **(B)** quantification of relative protein expression in experimental groups quantified by densitometry analysis; **(C)** representative Western blots for phospho-ATM, total ATM and β-actin as a loading control from DU145-Empty and DU145-LOX-PP cells subjected to IR (5 Gy); (D) the quantification of relative protein expression quantified by densitometry analysis; The experiments were repeated 3 times. Data are the averages of means of three independent experiments +/− SEM (n=3; * P<0.05, **p<0.01, *** P<0.001; student's t-test).

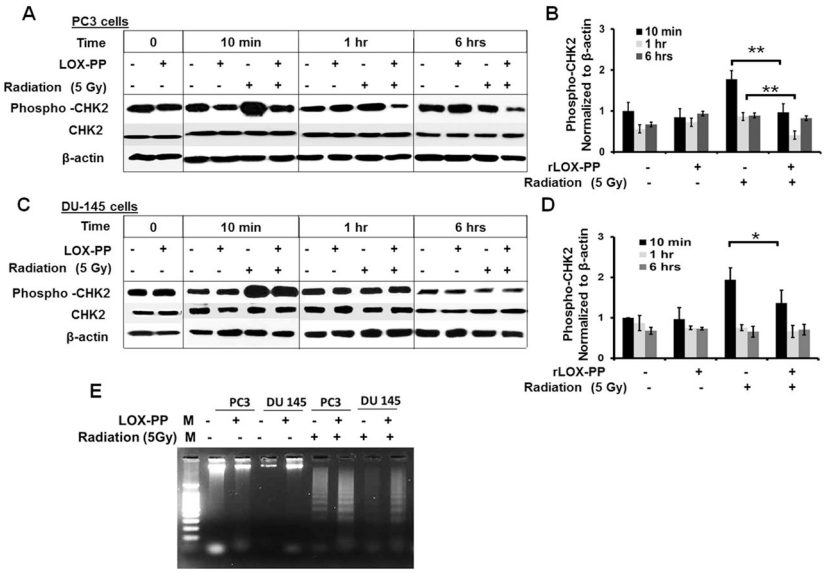

Figure 3. LOX-PP inhibits DNA damage induced CHK2 phosphorylation and DNA fragmentation detected by agarose gel electrophoresis

PC3 and DU145 cells were transduced with Empty- and rLOX-PP-expressing lentivirus particles and were cultured in 6-well plates and subjected to IR (5 Gy). Equal amounts of cell layer protein extracts from each cell extract (n=3) were pooled together and 40 μg aliquots of protein were evaluated for the expression of phospho-CHK2, total CHK2 and β-actin. The experiments were performed 3 times with different preparations of cells. **(A)** Representative Western blots for phospho-CHK2, total CHK2 and β-actin as a loading control from the PC3-Empty and PC3-LOX-PP cells subjected to IR (5 Gy); **(B)** the quantification of relative protein expression by densitometry analysis; **(C)** Western blot for phospho-CHK2, total CHK2 and β-actin as a loading control from the DU145-Empty and DU145-LOX-PP cells subjected to IR (5 Gy); **(D)** the quantification of relative protein expression by densitometry analysis. Experiments were performed 3 times. Data are the averages of means of three independent experiments +/− SEM (n=3; *, $P<0.05$; student's t-test). **(E)** PC3 and DU145 cells were transduced with Empty and rLOX-PP-expressing lentivirus particles, were cultured in 6-well plates and subjected to IR (5 Gy). Cells were harvested after 24 hrs for DNA isolation and subjected to 2% agarose gel electrophoresis in the presence of ethidum bromide and then visualized under UV light and photographed; (M) molecular weight marker.

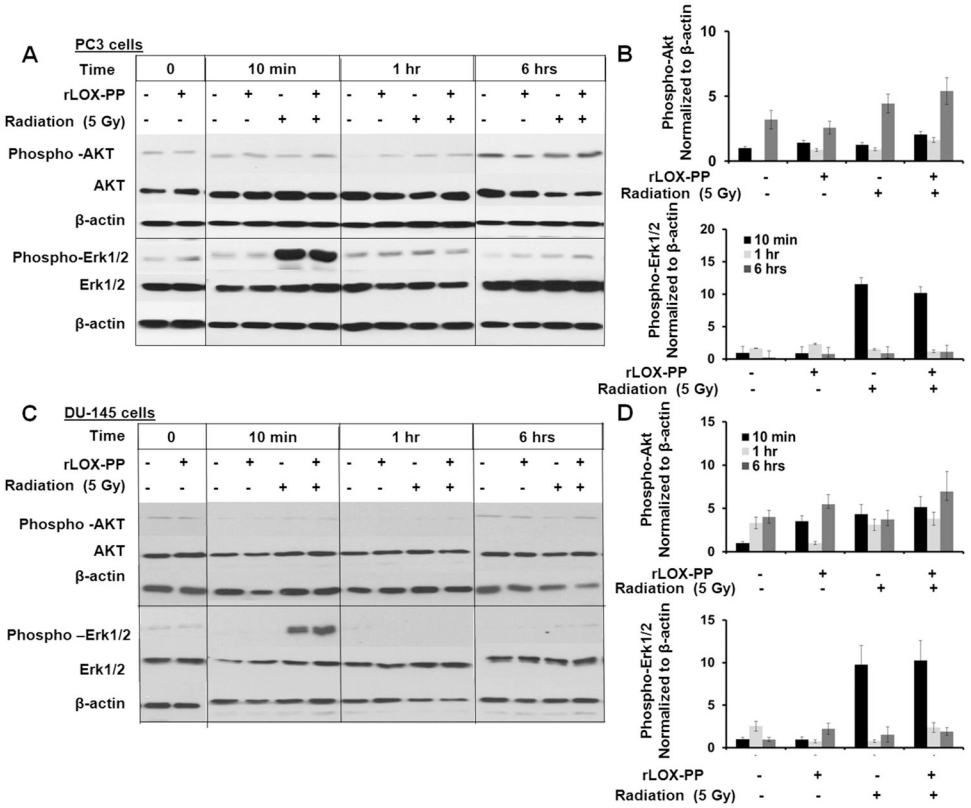

Figure 4. LOX-PP inhibition of IR induced DNA damage repair response is independent of its effect on Ras signaling pathways

PC3 and DU145 cells transduced with Empty and rLOX-PP-expressing lentivirus particles were plated in 6-well plates and subjected to IR (5 Gy). Equal amounts of protein extracts from each independent culture (n=3) were pooled and 40 μg samples were subjected to SDS PAGE and Western blotting to evaluate the expression of phospho-Akt, phospho ERK1/2, total AKT, total AKT and β-actin. The experiments were performed with 3 different preparations of cells. **(A)** Representative Western blots for phospho-AKT, total AKT and β-actin as a loading control and phospho ERK1/2, total ERK and β-actin from PC3-Empty and PC3-LOX-PP cells subjected to IR (5 Gy) **(B)** quantification of relative protein expression by densitometry analysis; **(C)** representative Western blots for phospho-AKT, total AKT and β-actin as a loading control and phospho ERK1/2, total ERK and β-actin from the PC3-Empty and PC3-LOX-PP cells from the DU145-Empty and DU145-LOX-PP cells subjected to IR (5 Gy) (D) the quantification of relative protein expression by densitometry analysis. Experiments were repeated 3 times. Data are the averages of means of three independent experiments +/− SEM (n=3).

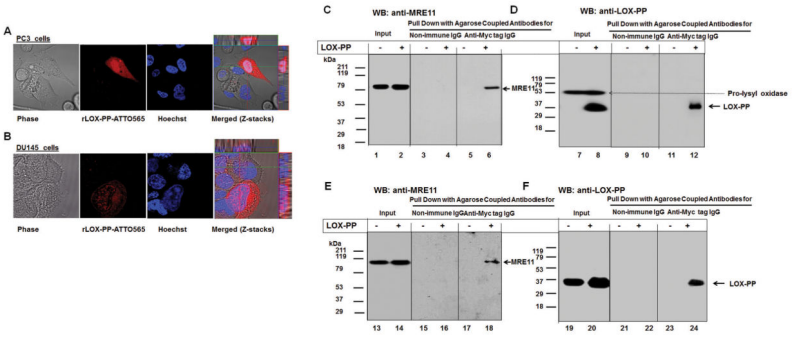

Figure 5. rLOX-PP nuclear localization in prostate cancer cell line PC3 (A) and DU145 (B), and LOX-PP interaction with MRE11 protein complexes PC3 cells (C) and DU145 cells (D)

For uptake studies, 30,000 PC3 and DU145 cells in F12K or DMEM media were cultured in chamber slides in standard media and were then replenished with serum-free F12K or DMEM media (0.1% BSA, 1 % penicillin-streptomycin) for 24 hrs. rLOX-PP labeled with ATTO565 (4 μg/ml rLOX-PP-ATTO565) was added as indicated and incubated for 36 hrs, and subjected to confocal microscopy by using Zeiss 710 dual scanner confocal microscope in a live cell imaging chamber at 37°C with 5% CO_2. **(A and B)** Confocal microscopy revealed apparent nuclear and cytoplasmic association of rLOX-PP in PC3 and DU145 cells, respectively. In each panel the images shown from left to right are phase contrast, rLOX-PP-ATTO565, Hoechst staining to label nuclei, and corresponding merged images showing in addition the 0.2 micrometer plane (Z-stack) derived from the indicated cross-section in the cell nucleus. For LOX-PP interaction studies (Panels C – F), PC3 (C and D) and DU145 (E and F) empty vector and rLOX-PP expressing PC3 and DU145 cells were cultured, extracted into non-denaturing cell lysis RIPA buffer. Cells were washed extensively with PBS, lysed and extracted with 500 μl non-denaturing cell lysis buffer (Profound c-Myc Tag IP/Co-IP kit; Thermo Scientific). Agarose beads with covalently bound non-immune IgG or anti-Myc-tag IgG antibody was added to samples and incubated overnight at 4° C to pull down rLOX-PP and any bound proteins. Resins were transferred to columns, washed, and then subjected to an acid elution protocol according to the manufacturer's instructions. **(C)** Western blot analysis of 5% input samples from PC3-Empty and from PC3-LOX-PP cells in lanes 1 and 2 demonstrates the presence of MRE11. Eluted samples from non-immune IgG agarose in lanes 3 and 4 and from anti-Myc-tag IgG in lanes 5 and 6 identify MRE11 only from cells expressing rLOX-PP and only in the anti-Myc tag IgG agarose pull down, as expected; **(D)** detection of immunoprecipitated rLOX-PP after stripping and re-probing with anti-LOX-PP antibody showing endogenous 50 kDa pro-lysyl oxidase in lanes 7 and 8, and rLOX-PP in lanes 8 and 12 only. **(E)** Western blot analysis of 5% input samples from DU145-Empty and from DU145-LOX-PP cells in lanes 13 and 14 demonstrates the presence of MRE11. Eluted samples from non-immune IgG agarose in lanes 15 and 16 and from anti-Myc-tag IgG in lanes 17 and 18 identify MRE11 only from cells expressing rLOX-PP and only in the anti-Myc tag IgG agarose pull down, as expected; **(F)** detection of immunoprecipitated rLOX-PP after stripping and re-probing with anti-LOX-PP antibody identified rLOX-PP in lane 24 only, as expected. The experiments were repeated 3 times each from protein extracts from 3 different batches of cells with the same outcomes.

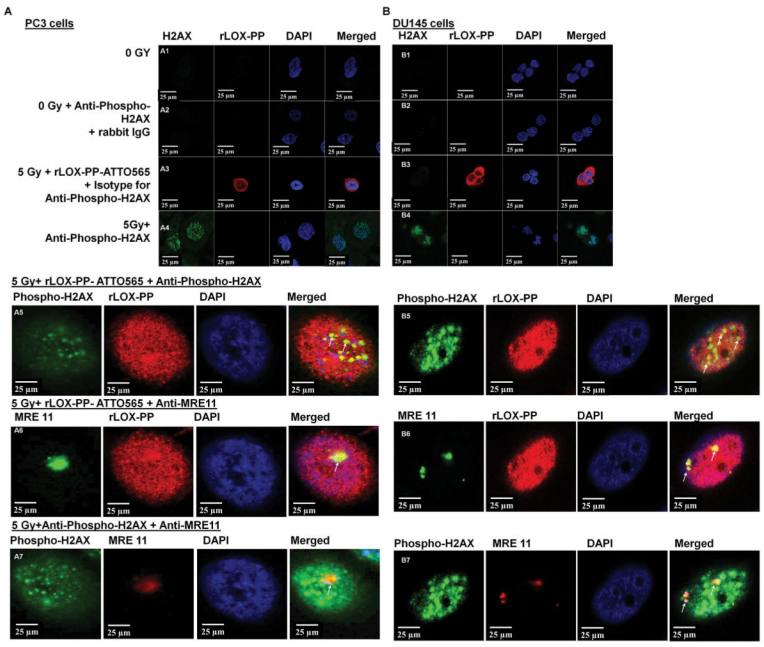

Figure 6. LOX-PP co-localizes with DNA repair foci in irradiated PC3 and DU145 cells

PC3 (A) or DU145 (B) cells were respectively cultured in chamber slides for 18 hrs in standard media with 10% serum, treated with labeled rLOX-PP (rLOX-PP-ATTO565) for 36 hrs for direct detection. Cells were subjected to 5 Gy IR. After 1 hour, irradiated and non-irradiated control cells were fixed, stained and subjected to confocal microscopy for rLOX-PP-ATTO565, phosphorylated-H2AX and MRE11 (Materials and Methods). **Row A1**, PC3 cells not treated with IR; **row A2**, PC3 cells no radiation control probed with anti-phosphorylated-H2AX; **row A3**, PC3 cells treated with IR in the presence of rLOX-PP-ATTO565, and probed with isotype non-immune antibody (negative control for anti-H2AX antibody), **row A4**, PC3 cells treated with IR in the absence of rLOX-PP-ATTO565, and probed with anti-phosphorylated-H2AX antibody; **row A5**, PC3 cells treated with IR and rLOX-PP-ATTO565, and probed with anti-phosphorylated-H2AX- and visualized for presence of rLOX-PP-ATTO565; **row A6**, PC3 cells treated with IR and rLOX-PP, and probed with MRE 11- and visualized for presence of rLOX-PP-ATTO565, and **row A7**, PC3 cells treated with IR and rLOX-PP-ATTO565, and probed with anti-phosphorylated-H2AX and MRE 11 antibody. **Row B1**; DU145 cells not treated with IR; **row B2**, DU145 cells not treated with IR but probed with anti-phosphorylated-H2AX antibody to detect endogenous expression of phosphorylated-H2AX independent of radiation treatment; **row B3**, DU145 cells treated with IR in the presence of rLOX-PP-ATTO565, and probed with isotype control antibody for anti-phosphorylated-H2AX; **row B4**, DU145 cells treated with IR in the absence of rLOX-PP-ATTO565, and probed for phosphorylated-H2AX; **row B5**, DU145 cells treated with IR and rLOX-PP-ATTO565, and probed with anti-phosphorylated-H2AX and visualized for presence of rLOX-PP-ATTO565; **row B6**, DU145 cells treated with IR and rLOX-PP-ATTO565, and probed with MRE 11- and anti-LOX-PP antibody; and **row B7**, DU145 cells treated with IR and rLOX-PP-ATTO565, and probed with anti-phosphorylated-H2AX and MRE 11 antibody.

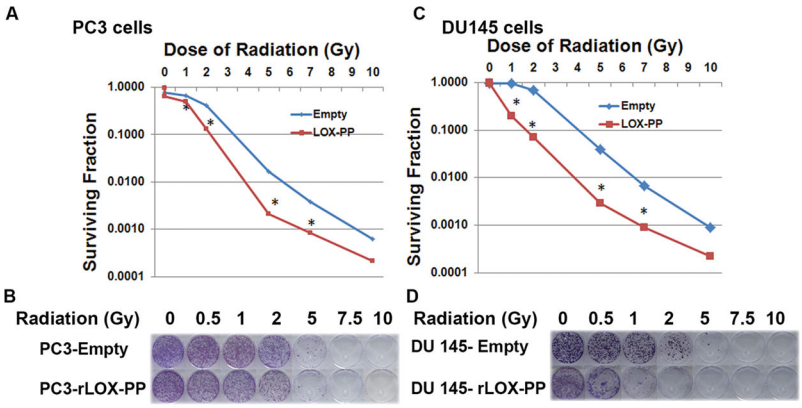

Figure 7. LOX-PP inhibits clonogenic survival in response to different doses of radiation

PC3 and DU145 cells were transduced with Empty- and rLOX-PP-expressing lentiviruses and cells were grown under standard cell culture conditions and subjected to 0, 0.5,1, 2, 3, 5, 7.5 and 10 Gy of ionizing radiation. Cells were sorted to exclude dead cells and live cells were plated at 5000 or 1000 live cells in 6-well cell culture plates. Colonies were allowed to grow for 14 days, and cultures were then fixed and then stained with crystal violet. The survival fraction was calculated as described in Materials and Methods. **(A)** PC3-Empty or PC3-LOX-PP cells surviving fraction as a function of radiation dose; **(B)** respective images of cells stained with 0.5% crystal violet; **(C)** DU145-Empty or DU145-LOX-PP cells surviving fraction as a function of radiation dose; **(D)** respective images stained with 0.5% crystal violet; (n=6); * $p<0.05$; student's t-test from one representative experiment of three performed with the same outcomes.